PKA regulation of neuronal function requires the dissociation of catalytic subunits from regulatory subunits

Wei-Hong Xiong, Maozhen Qin, and Haining Zhong

Vollum Institute, Oregon Health & Science University, Portland, OR 97239, USA

Correspondence should be addressed to H.Z. (email: zhong@ohsu.edu).

Haining Zhong, Ph.D.
Vollum Institute, Oregon Health & Science University
3181 SW Sam Jackson Park Road, L474
Portland, Oregon 97239
U.S.A.
(503) 494-5089 / zhong@ohsu.edu

Key words: cAMP-dependent kinase / protein kinase A (PKA); two-photon imaging; norepinephrine; shRNA knockdown; late-phase structural long-term potentiation; AMPA and NMDA-mediated synaptic transmission.

Abstract

Protein kinase A (PKA) plays essential roles in diverse cellular functions. However, the spatiotemporal dynamics of endogenous PKA upon activation remain debated. The classical model predicts that PKA catalytic subunits dissociate from regulatory subunits in the presence of cAMP, whereas a second model proposes that catalytic subunits remain associated with regulatory subunits following physiological activation. Here we report that different PKA subtypes, as defined by the regulatory subunit, exhibit distinct subcellular localization at rest in CA1 neurons of cultured hippocampal slices. Nevertheless, when all tested PKA subtypes are activated by norepinephrine, presumably via the β-adrenergic receptor, catalytic subunits translocate to dendritic spines but regulatory subunits remain unmoved. These differential spatial dynamics between the subunits indicate that at least a significant fraction of PKA dissociates. Furthermore, PKA-dependent regulation of synaptic plasticity and transmission can be supported only by wildtype, dissociable PKA, but not by inseparable PKA. These results indicate that endogenous PKA regulatory and catalytic subunits dissociate to achieve PKA function in neurons.

31 **Introduction**

32 Cyclic adenosine monophosphate (cAMP)-dependent kinase, or protein kinase A (PKA),
33 regulates diverse critical functions in nearly all mammalian cells, including neurons. PKA is
34 a tetrameric protein consisting of two regulatory subunits (PKA-Rs) and two catalytic
35 subunits (PKA-Cs) (Francis and Corbin, 1994; Johnson et al., 2001). In the inactive state,
36 each PKA-R binds to and inhibits a PKA-C. Binding of cAMP to PKA-R activates PKA-C.
37 However, there are different proposals on the molecular events that follow activation.

38 For decades, PKA-C is thought to dissociate from PKA-R upon cAMP binding (Beavo
39 et al., 1974; Francis and Corbin, 1994; Gold, 2019; Johnson et al., 2001; Reimann et al.,
40 1971). Freed PKA-C molecules then move to phosphorylate their substrates. However, a
41 small number of studies (reviewed in Gold, 2019), including two notable recent
42 publications (Smith et al., 2017, 2013), propose an alternative model, in which
43 physiological concentrations of cAMP can activate PKA-C but do not result in its
44 dissociation from PKA-R. Testing these two models will not only elucidate the biophysical
45 mechanism of PKA activation, but also have distinct implications in how PKA may achieve
46 its specificity, which is thought to rely on spatial compartmentalization (Wong and Scott,
47 2004).

48 We have previously found that the majority of type IIβ PKA, as defined by PKA-R, is
49 anchored to microtubules in the dendritic shaft of hippocampal CA1 pyramidal neurons
50 where PKA-RIIβ is bound to the abundant microtubule associated protein MAP-2 (Zhong et
51 al., 2009). Upon activation of the β-adrenergic receptor with norepinephrine, a fraction of
52 PKA-C dissociated from PKA-RIIβ (Tillo et al., 2017). The freed PKA-C redistributed into

53 dendritic spines, whereas PKA-RIIβ remained anchored at the dendritic shaft (Tillo et al.,
54 2017; Xiong et al., 2021). These results are consistent with the classical PKA activation
55 model. However, recent studies suggest that PKA-Rs other than PKA-RIIβ may be the more
56 abundant isoforms in CA1 neurons (Church et al., 2021; Ilouz et al., 2017; Weisenhaus et al.,
57 2010). It remains untested whether these PKA isoforms dissociate upon physiologically
58 relevant stimulations in neurons.

59 Here, we examined whether PKA-C dissociates from the major PKA-R isoforms,
60 PKA-RIβ and PKA-RIIα, in CA1 neurons. The rescue of function following knockdown of
61 PKA-C was compared between wildtype dissociable PKA and an inseparable PKA variant in
62 which PKA-C is covalently linked to PKA-R. The result supports the classical model of PKA
63 activation via dissociation.

64 **Results**

65 Recent studies have suggested that PKA-RIIα and PKA-RIβ may be the prevalent
66 isoforms in hippocampal CA1 neurons. Therefore, we co-expressed C-terminally EGFP
67 tagged PKA-C (PKA-C-EGFP) (Tillo et al., 2017; Zhong et al., 2009) and a cytosolic marker
68 (mCherry) with either PKA-RIIα or PKA-RIβ in CA1 neurons of organotypic hippocampal
69 slice cultures (Figs. 1A and 1B, upper left panels). At rest, PKA-C-EGFP exhibited a
70 distribution that was dependent on the co-expressed PKA-R: when co-expressed with PKA-
71 RIIα, PKA-C was enriched in dendritic shafts; when co-expressed with PKA-RIβ, PKA-C was
72 more evenly distributed (quantified using the spine enrichment indexes, or SEI, see
73 Methods) (Fig. 1C). This distribution was independent of the expression level (rest

74 conditions in Figure S1) and largely resembled that of the corresponding PKA-R (Figs. 1A-
75 1C).

76 Notably, upon application of norepinephrine (10 μM), PKA-C of both subtypes
77 translocated to dendritic spines, but the subcellular localization of PKA-Rs remained
78 unchanged (Figs. 1D & 1E). This differential re-distribution between PKA-C and PKA-R was
79 more prominent following activation with forskolin (25 μM) and IBMX (50 μM). The
80 translocation of PKA-C was independent of the expression level and the effect remained
81 when extrapolating to the zero-overexpression level using a linear fit (Figure S1). These
82 results can only be explained if at least a fraction of PKA-C dissociated from both PKA-RIIα
83 and PKA-RIβ when a physiological stimulant was used. Together with our earlier results
84 regarding PKA-C/PKA-RIIβ, we conclude that PKA-C dissociates from PKA-R with
85 physiologically relevant stimuli.

86 Next, we asked whether PKA regulation of neuronal function is dependent on the
87 dissociation of PKA-C from PKA-R. A key experiment supporting the non-dissociating PKA
88 activation model was that PKA regulation of cell growth could be sustained by a construct
89 in which PKA-C was fused to PKA-RIIα in one polypeptide chain via a flexible linker (named
90 R-C; Fig. 2A) (Smith et al., 2017). We therefore asked whether this R-C construct could
91 support PKA regulation of neuronal function. When R-C-EGFP was expressed in CA1
92 neurons, this construct exhibited a distribution highly similar to that of RIIα (Figs. 2B and
93 2C). The tendency of this construct to translocate to the spine was largely diminished
94 compared to PKA-C-EGFP co-expressed with wildtype, unlinked PKA-RIIα (Fig. 2D),

95 indicating that the catalytic subunit in R-C was indeed inseparable from the regulatory
96 subunit.

97 To evaluate the function of R-C, a previously established shRNA construct was used
98 to selectively knock down PKA-Cα in CA1 neurons in cultured hippocampal slices (Tillo et
99 al., 2017). Given that PKA activation is required for the late phase of long-term potentiation
100 (L-LTP) (Abel et al., 1997), we examined the structural LTP of individual dendritic spines of
101 CA1 neurons elicited by focal two-photon glutamate uncaging (Fig. 3) (Matsuzaki et al.,
102 2004). The shRNA knockdown of PKA-C resulted in attenuated LTP at 90 min after
103 induction (Figs. 3A–3C). This attenuation was not observed when a control shRNA against
104 LacZ was expressed (Fig. 3C). The attenuated structural LTP was rescued by co-expression
105 of shRNA-resistant wild-type PKA-C-EGFP together with PKA-RIIα (Figs. 3A–3C). However,
106 the R-C construct in which PKA-C was also resistant to shRNA knockdown but could not
107 leave PKA-RIIα failed to rescue the phenotype.

108 PKA activity has also been shown to regulate synaptic transmission. We therefore
109 examined evoked AMPA and NMDA receptor (AMPAR and NMDAR, respectively) currents
110 in paired, transfected and adjacent untransfected CA1 neurons in cultured hippocampal
111 slices. As shown previously (Tillo et al., 2017; Xiong et al., 2021), neurons expressing the
112 shRNA construct against PKA-C exhibited significantly lower AMPAR currents (Fig. 4A), but
113 not NMDAR currents (Fig. 4B). As a result, the AMPAR/NMDAR current ratio was also
114 reduced (Fig. 4C). The deficits were rescued by co-expression of shRNA-resistant, wild-type
115 dissociable PKA-C-EGFP and PKA-RIIα (Fig. 4). However, the inseparable R-C construct

116 failed to rescue the phenotype. Taken together, the R-C construct did not support normal
117 PKA-dependent synaptic function.

118 **Discussion**

119 Our results indicate that at least a fraction of PKA-C molecules dissociate from all
120 tested PKA-R isoforms, including Iβ, IIα and previously tested IIβ, when activated by
121 physiological stimuli. Given that PKA activity increases by two orders of magnitude when
122 dissociated from PKA-R (Miyamoto et al., 1969), even a small fraction of PKA-C dissociation
123 will result in a marked increase of PKA kinase activity. These results corroborate the
124 observations in intact non-neuronal cells that used FRET imaging and biochemical
125 measurements, respectively (Walker-Gray et al., 2017; Zaccolo et al., 2000). Furthermore,
126 PKA-C that is covalently linked to PKA-RIIα cannot functionally replace wildtype PKA for
127 normal neuronal transmission or plasticity. Although this R-C construct has been shown to
128 functionally replace endogenous PKA in terms of supporting the growth of a heterologous
129 cell line (Smith et al., 2017), it cannot support all necessary PKA functions. Overall, we
130 conclude that PKA-C dissociation from PKA-R is essential for PKA regulation of neuronal
131 function. Additionally, PKA specificity is mediated by spatial compartmentalization (Wong
132 and Scott, 2004). This is likely mediated by mechanism downstream of PKA dissociation,
133 such as membrane tethering of freed PKA-C or its buffering by extra PKA-Rs (Gaffarogullari
134 et al., 2011; Tillo et al., 2017; Walker-Gray et al., 2017; Zhang et al., 2015).

135 In addition, this study shows that PKA distribution in neuronal dendrites at the
136 resting state is subtype dependent. PKA-RIIα is enriched in dendritic shaft in a way similar
137 to PKA-RIIβ, likely via its interaction with the abundant microtubule binding protein MAP2

138 (Tillo et al., 2017; Vallee et al., 1981). Note that this observation does not exclude the
139 importance a small fraction of PKA being anchored to synaptic sites via other PKA binding
140 proteins. In contrast, PKA-RIβ is more evenly distributed between spine and dendrites.
141 These observations establish a spatial organizational base for understanding subtype-
142 specific PKA function in neurons.

143 This study also demonstrates that PKA is essential for long-term structural LTP of
144 individual spines. PKA has been shown to facilitate the induction of LTP (i.e.,
145 metaplasticity) (Thomas et al., 1996; Zhong et al., 2009), and is required for the
146 maintenance of L-LTP (Abel et al., 1997), as assayed using electrophysiological recording of
147 postsynaptic currents. However, it has been suggested that the structural and synaptic
148 current changes may not be causally linked (Kopec et al., 2006). Our results fill the gap to
149 show that PKA is also required for maintaining the late phase of structural LTP.

150 **Materials and Methods**

151 **Plasmid constructs**

152 Constructs were made using standard mutagenesis and subcloning methods. All previously
153 unpublished constructs and their sequences will be submitted to Addgene. In the R-C
154 construct, mouse PKA-RIIα and PKA-Cα were fused via a linker with residues
155 WDPGSGSLEAGCKNFFPRSFTSCGSLEGGSAAA that were previously used (Smith et al.,
156 2017).

157 **Organotypic hippocampal slice cultures and transfections**

158 Cultured rat hippocampal slices were prepared from P6 – P8 (typically P7) pups, as
159 described previously (Stoppini et al., 1991; Zhong et al., 2009). Animal experiments were
160 performed in accordance with the Guide for the Care and Use of Laboratory Animals of the
161 National Institutes of Health, and were approved by the Institutional Animal Care and Use
162 Committee (IACUC) of the Oregon Health & Science University (#IP00002274). cDNA
163 constructs were transfected after 1.5–3 weeks *in vitro* via the biolistic gene transfer
164 method using the Helios gene gun and 1.6 μm gold beads (Fig. 1) or, where long-term
165 expression (~ 1 week) was required, with single-cell electroporation (Fig. 2) (Otmakhov
166 and Lisman, 2012).

167 **Two-photon imaging and two-photon glutamate uncaging**

168 A custom built two-photon microscope based on an Olympus BW51WI microscope body
169 was used. Laser beams from two different Ti:Sapphire lasers (Maitai, Newport) were
170 aligned to allow for simultaneous two-photon excitation and photoactivation. Laser
171 intensities were controlled by Pockels cells (Conoptics). Imaging and photoactivation were

172 controlled by ScanImage (Vidrio Tech) (Pologruto et al., 2003). Slices were perfused during
173 imaging in gassed artificial cerebral spinal fluid (ACSF) containing (mM) 127 NaCl, 25
174 $NaHCO_3$, 25 D-glucose, 2.5 KCl, 4 $MgCl_2$, 4 $CaCl_2$, and 1.25 NaH_2PO_4 with 0.5 μM
175 tetrodotoxin (TTX). mEGFP fluorescence (green) was unmixed from that of the cytosolic
176 marker (mCherry or DsRed Express) using a dichroic (Chroma 565DCXR) and band-pass
177 filters (Chroma HQ510/70 for green and Semrock FF01-630/92 for red).

178 For single-spine structural LTP experiments, 2.25 mM MNI-caged-L-glutamate
179 (Tocris) was added to ACSF containing 4 mM calcium, 0.05 mM magnesium, 1 μM TTX and
180 4 μM 2-chloroadenosine, as previously described (Harvey et al., 2008a). To trigger
181 structural plasticity, 30 pulses of 4-ms 16-mW (at back focal plane) 720-nm laser light
182 were delivered to the spine head at 0.5 Hz.

183 Image analysis was performed using custom software written in MATLAB called
184 *SI_View* (https://github.com/HZhongLab/SI_View) (Ma et al., 2022). Using the software,
185 regions of interest (ROIs) were manually drawn to isolate spines or their immediately
186 adjacent dendritic shaft. Only the spines well isolated from the dendrite laterally
187 throughout the entire experiments were included. Spine enrichment index was calculated
188 as:

189 $$SEI = \log_2[(F_{green}/F_{red})_{spine}/(F_{green}/F_{red})_{shaft}]$$

190 in which F is the average fluorescence intensity in an ROI.

191 The expression level was estimated by the maximal intensity from thick apical
192 dendrite near the soma (typically 50-100 μm) similar to previously described (Harvey et

193 al., 2008b; Tillo et al., 2017). To minimize the influence of noise, a line of 9 pixels (pixel size
194 ~0.04 μm) thick was manually drawn transecting the dendrite through the visually
195 identified, brightest region. The line profile was further smoothened by 5 pixels along the
196 line and baseline subtracted before determining the maximal value. To combine
197 measurements from different hardware configuration (e.g., different microscopes), the data
198 from each configuration and experiment were internally corrected for laser stimulation
199 intensity and then normalized to the average of all data under the same condition.

200 **Electrophysiology**

201 Whole-cell voltage-clamp recordings were performed using a MultiClamp 700B amplifier
202 (Molecular Devices). Electrophysiological signals were filtered at 2 kHz and digitized and
203 acquired at 20 kHz using custom software written in MATLAB. Slices were perfused with
204 artificial cerebrospinal fluid containing 4 mM Ca and 4 mM Mg. The internal solution
205 contained (in mM) 132 Cs-gluconate, 10 HEPES, 10 Na-phosphocreatine, 4 MgCl2, 4 Na2-
206 ATP, 0.4 Na-GTP, 3 Na-ascorbate, 3 QX314, and 0.2 EGTA with an osmolarity of 295
207 mOsmol/kg. The junction potential was calculated to be -17 mV using a built-in function in
208 the Clampfit software (Molecular Devices). Several less abundant anions (phosphocreatine,
209 ATP, GTP and ascorbate) were omitted in the calculation due to lack of data in the program.
210 The Cl reversal potential was -75 mV.

211 To reduce recurrent activities, cultured hippocampal slices were cut on both sides of
212 CA1 and 4 μM 2-chloroadenosine (Sigma) was present in all recording experiments. 10 μM
213 GABAzine (SR 95531, Tocris) was also included to suppress GABA currents. For electrical
214 stimulation, a bipolar, θ-glass stimulating electrode (Warner Instruments) was positioned

215 in the stratum radiatum 100–150 μm lateral to the recorded neuron. For all recordings, a
216 transfected neuron and an untransfected neuron located within 50 μm of each other were
217 sequentially recorded without repositioning the stimulation electrode. Measurements were
218 carried out on averaged traces from approximately 20 trials under each condition. For
219 AMPAR currents, the cells were held at -60 mV (before correcting for the junction
220 potential) and the current was measured as the baseline-subtracted peak current within a
221 window of 2–50 ms after electric stimulation. For NMDAR currents, the average currents at
222 140 to 160 ms after stimulation were used when the cells were held at +55 mV (before
223 correcting for the junction potential)

224 **Data analysis, presentation, and statistics**

225 Quantification and statistical tests were performed using custom software written in
226 MATLAB. Averaged data are presented as mean ± s.e.m., unless noted otherwise. p values
227 were obtained from one-way ANOVA tests, unless noted otherwise. In all figures, *: $p \leq 0.05$
228 and is considered statistically significant after Bonferroni correction for multiple tests, **: p
229 ≤ 0.01, and ***: $p \leq 0.001$.

230

Acknowledgements

We thank all members of the Mao and Zhong laboratories at the Vollum Institute for constructive discussions. We thank Drs John Williams and Michael Muniak for critical comments and edits on the manuscript. This work was supported by two NIH BRAIN Initiative awards to H.Z. (U01NS094247 and R01NS127013).

Author contributions

H.Z. conceived the project. W.X. and H.Z. designed the experiments. W.X. and H.Z. performed the experiments and data analyses. M.Q. produced critical reagents used in the experiments. H.Z. wrote the manuscript.

Competing interests

The authors declare no competing interests.

244 **References**

245 Abel T, Nguyen P V., Barad M, Deuel TAS, Kandel ER, Bourtchouladze R. 1997. Genetic
246 demonstration of a role for PKA in the late phase of LTP and in hippocampus-based
247 long-term memory. *Cell* **88**:615–626. doi:10.1016/S0092-8674(00)81904-2

248 Beavo JA, Bechtel PJ, Krebs EG. 1974. Activation of protein kinase by physiological
249 concentrations of cyclic AMP. *Proc Natl Acad Sci U S A*. doi:10.1073/pnas.71.9.3580

250 Church TW, Tewatia P, Hannan S, Antunes J, Eriksson O, Smart TG, Kotaleski JH, Gold MG.
251 2021. Akap79 enables Calcineurin to directly suppress protein Kinase a activity. *Elife*
252 **10**. doi:10.7554/eLife.68164

253 Francis SH, Corbin JD. 1994. Structure and Function of Cyclic Nucleotide-Dependent
254 Protein Kinases. *Annu Rev Physiol*. doi:10.1146/annurev.ph.56.030194.001321

255 Gaffarogullari EC, Masterson LR, Metcalfe EE, Traaseth NJ, Balatri E, Musa MM, Mullen D,
256 Distefano MD, Veglia G. 2011. A myristoyl/phosphoserine switch controls cAMP-
257 dependent protein kinase association to membranes. *J Mol Biol*.
258 doi:10.1016/j.jmb.2011.06.034

259 Gold MG. 2019. Swimming regulations for protein kinase A catalytic subunit. *Biochem Soc*
260 *Trans*. doi:10.1042/BST20190230

261 Harvey CD, Yasuda R, Zhong H, Svoboda K. 2008a. The spread of Ras activity triggered by
262 activation of a single dendritic spine. *Science (80-)* **321**:136–140.
263 doi:10.1126/science.1159675

264 Harvey CD, Yasuda R, Zhong H, Svoboda K. 2008b. The spread of Ras activity triggered by
265 activation of a single dendritic spine. *Science (80-)* **321**:136–140.
266 doi:10.1126/science.1159675

267 Ilouz R, Lev-Ram V, Bushong EA, Stiles TL, Friedmann-Morvinski D, Douglas C, Goldberg G,
268 Ellisman MH, Taylor SS. 2017. Isoform-specific subcellular localization and function of
269 protein kinase a identified by mosaic imaging of mouse brain. *Elife* **6**.
270 doi:10.7554/eLife.17681

271 Johnson DA, Akamine P, Radzio-Andzelm E, Madhusudan, Taylor SS. 2001. Dynamics of
272 cAMP-dependent protein kinase. *Chem Rev*. doi:10.1021/cr000226k

273 Kopec CD, Li B, Wei W, Boehm J, Malinow R. 2006. Glutamate receptor exocytosis and spine
274 enlargement during chemically induced long-term potentiation. *J Neurosci* **26**:2000–
275 2009. doi:10.1523/JNEUROSCI.3918-05.2006

276 Ma L, Day-Cooney J, Benavides OJ, Muniak MA, Qin M, Ding JB, Mao T, Zhong H. 2022.
277 Locomotion activates PKA through dopamine and adenosine in striatal neurons.
278 *Nature* **611**:762–768. doi:10.1038/s41586-022-05407-4

279 Matsuzaki M, Honkura N, Ellis-Davies GCR, Kasai H. 2004. Structural basis of long-term
280 potentiation in single dendritic spines. *Nature* **429**:761–766.
281 doi:10.1038/nature02617

282 Miyamoto E, Kuo JF, Greengard P. 1969. Cyclic nucleotide-dependent protein kinases. 3.
283 Purification and properties of adenosine 3',5'-monophosphate-dependent protein

284 kinase from bovine brain. *J Biol Chem* **244**:6395–6402.

285 Otmakhov N, Lisman J. 2012. Measuring CaMKII concentration in dendritic spines. *J*
286 *Neurosci Methods*. doi:10.1016/j.jneumeth.2011.09.022

287 Pologruto TA, Sabatini BL, Svoboda K. 2003. ScanImage: Flexible software for operating
288 laser scanning microscopes. *Biomed Eng Online* **2**:13. doi:10.1186/1475-925X-2-13

289 Reimann EM, Brostrom CO, Corbin JD, King CA, Krebs EG. 1971. Separation of regulatory
290 and catalytic subunits of the cyclic 3′, 5′-adenosine monophosphate-dependent
291 protein kinase(s) of rabbit skeletal muscle. *Biochem Biophys Res Commun* **42**.
292 doi:10.1016/0006-291X(71)90086-6

293 Smith FD, Esseltine JL, Nygren PJ, Veesler D, Byrne DP, Vonderach M, Strashnov I, Eyers CE,
294 Eyers PA, Langeberg LK, Scott JD. 2017. Local protein kinase A action proceeds
295 through intact holoenzymes. *Science (80-)* **356**. doi:10.1126/science.aaj1669

296 Smith FD, Reichow SL, Esseltine JL, Shi D, Langeberg LK, Scott JD, Gonen T. 2013. Intrinsic
297 disorder within an AKAP-protein kinase A complex guides local substrate
298 phosphorylation. *Elife* **2013**. doi:10.7554/eLife.01319.001

299 Stoppini L, Buchs PA, Muller D. 1991. A simple method for organotypic cultures of nervous
300 tissue. *J Neurosci Methods*. doi:10.1016/0165-0270(91)90128-M

301 Thomas MJ, Moody TD, Makhinson M, O'Dell TJ. 1996. Activity-dependent β-adrenergic
302 modulation of low frequency stimulation induced LTP in the hippocampal CA1 region.
303 *Neuron* **17**:475–482. doi:10.1016/S0896-6273(00)80179-8

304 Tillo SE, Xiong WH, Takahashi M, Miao S, Andrade AL, Fortin DA, Yang G, Qin M, Smoody BF,
305 Stork PJS, Zhong H. 2017. Liberated PKA Catalytic Subunits Associate with the
306 Membrane via Myristoylation to Preferentially Phosphorylate Membrane Substrates.
307 *Cell Rep* **19**:617–629. doi:10.1016/j.celrep.2017.03.070

308 Vallee RB, DiBartolomeis MJ, Theurkauf WE. 1981. A protein kinase bound to the projection
309 portion of MAP 2 (microtubule-associated protein 2). *J Cell Biol* **90**.
310 doi:10.1083/jcb.90.3.568

311 Walker-Gray R, Stengel F, Gold MG. 2017. Mechanisms for restraining cAMP-dependent
312 protein kinase revealed by subunit quantitation and cross-linking approaches. *Proc*
313 *Natl Acad Sci U S A* **114**:10414–10419. doi:10.1073/pnas.1701782114

314 Weisenhaus M, Allen ML, Yang L, Lu Y, Nichols CB, Su T, Hell JW, Mcknight GS. 2010.
315 Mutations in AKAP5 disrupt dendritic signaling complexes and lead to
316 electrophysiological and behavioral phenotypes in mice. *PLoS One* **5**.
317 doi:10.1371/journal.pone.0010325

318 Wong W, Scott JD. 2004. AKAP signalling complexes: Focal points in space and time. *Nat*
319 *Rev Mol Cell Biol*. doi:10.1038/nrm1527

320 Xiong WH, Qin M, Zhong H. 2021. Myristoylation alone is sufficient for PKA catalytic
321 subunits to associate with the plasma membrane to regulate neuronal functions. *Proc*
322 *Natl Acad Sci U S A* **118**. doi:10.1073/pnas.2021658118

323 Zaccolo M, De Giorgi F, Cho CY, Feng L, Knapp T, Negulescu PA, Taylor SS, Tsien RY, Pozzan

324 T. 2000. A genetically encoded, flourescent indicator for cyclic AMP in living cells. *Nat*
325 *Cell Biol* **2**:25–29. doi:10.1038/71345

326 Zhang P, Ye F, Bastidas AC, Kornev AP, Wu J, Ginsberg MH, Taylor SS. 2015. An Isoform-
327 Specific Myristylation Switch Targets Type II PKA Holoenzymes to Membranes.
328 *Structure*. doi:10.1016/j.str.2015.07.007

329 Zhong H, Sia GM, Sato TR, Gray NW, Mao T, Khuchua Z, Huganir RL, Svoboda K. 2009.
330 Subcellular Dynamics of Type II PKA in Neurons. *Neuron* **62**:363–374.
331 doi:10.1016/j.neuron.2009.03.013

332

333 **Figures and figure legends**

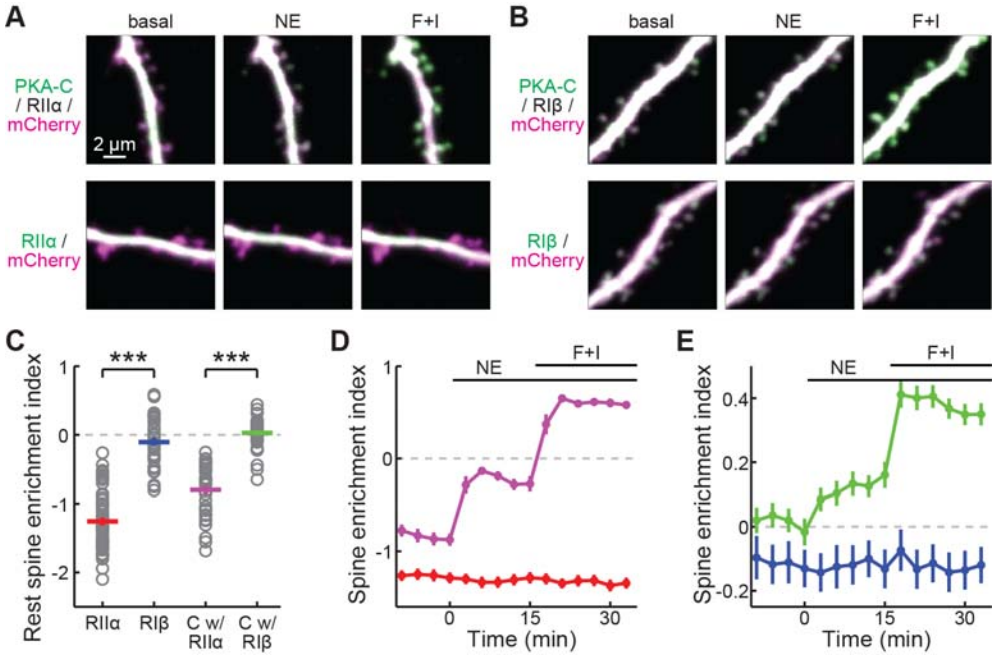

334

335 **Figure 1**. PKA-C but not PKA-R redistributes to spines upon activation. (A, B)

336 Representative two-photon images of PKA-C-EGFP co-expressed with PKA-RIIα or PKA-RIβ

337 at rest, or in the presence of norepinephrine (NE) or forskolin and IBMX (F + I). mCherry

338 (magenta) was co-expressed to reveal the neuronal morphology. (C–E) Quantification and

339 comparison of the spine enrichment index at the resting state (C) and upon activation (D &

340 E). As in panel C from left to right, n (spines/neurons) = 53/11, 34/7, 33/6, and 36/7.

341

342

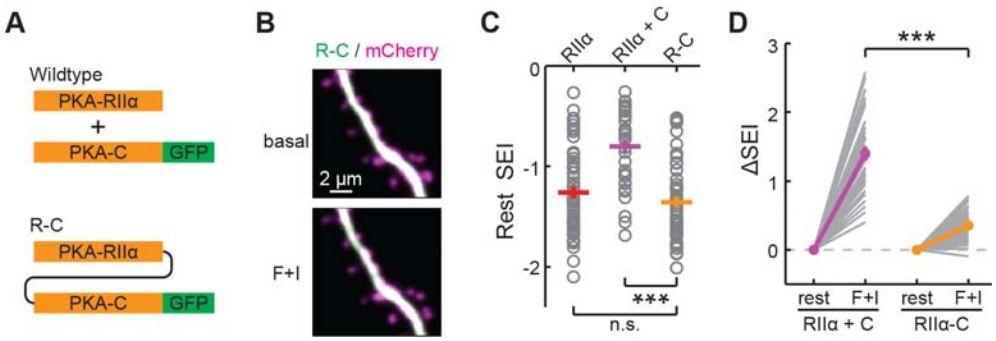

343 **Figure 2**. Characterization of the inseparable R-C. (A) Schematic of wildtype PKA versus R-

344 C. In both cases PKA-C was C-terminally tagged by mEGFP. (B–C) Representative images

345 (B), quantifications of resting distribution (C), and the distribution change upon

346 stimulation by forskolin and IBMX (D) of R-C compared to PKA-RIIα-EGFP and co-

347 expressed PKA-C-EGFP/PKA-RIIα. RIIα and RIIα+C data are from Fig. 1C. n

348 (spines/neurons) = 48/10.

349

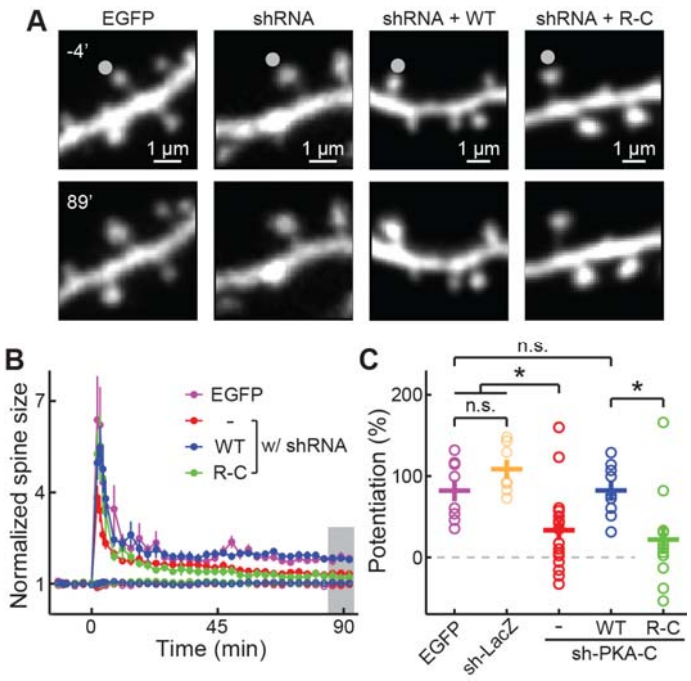

350

351 **Figure 3**. PKA regulation of synaptic plasticity cannot be sustained by an inseparable PKA

352 variant. (A–C) Representative image (A), time course (B), and the degree of potentiation (C)

353 at the indicated timepoints in panel B of single-spine LTP experiments as triggered by focal

354 glutamate uncaging at the marked spines (gray dot). In panel B, both stimulated spines

355 (solid circles) and non-stimulated control spines (open circles) are shown. As in panel C

356 from left to right, n (spines, each from a different neuron) = 8, 7, 17, 11, 9.

357

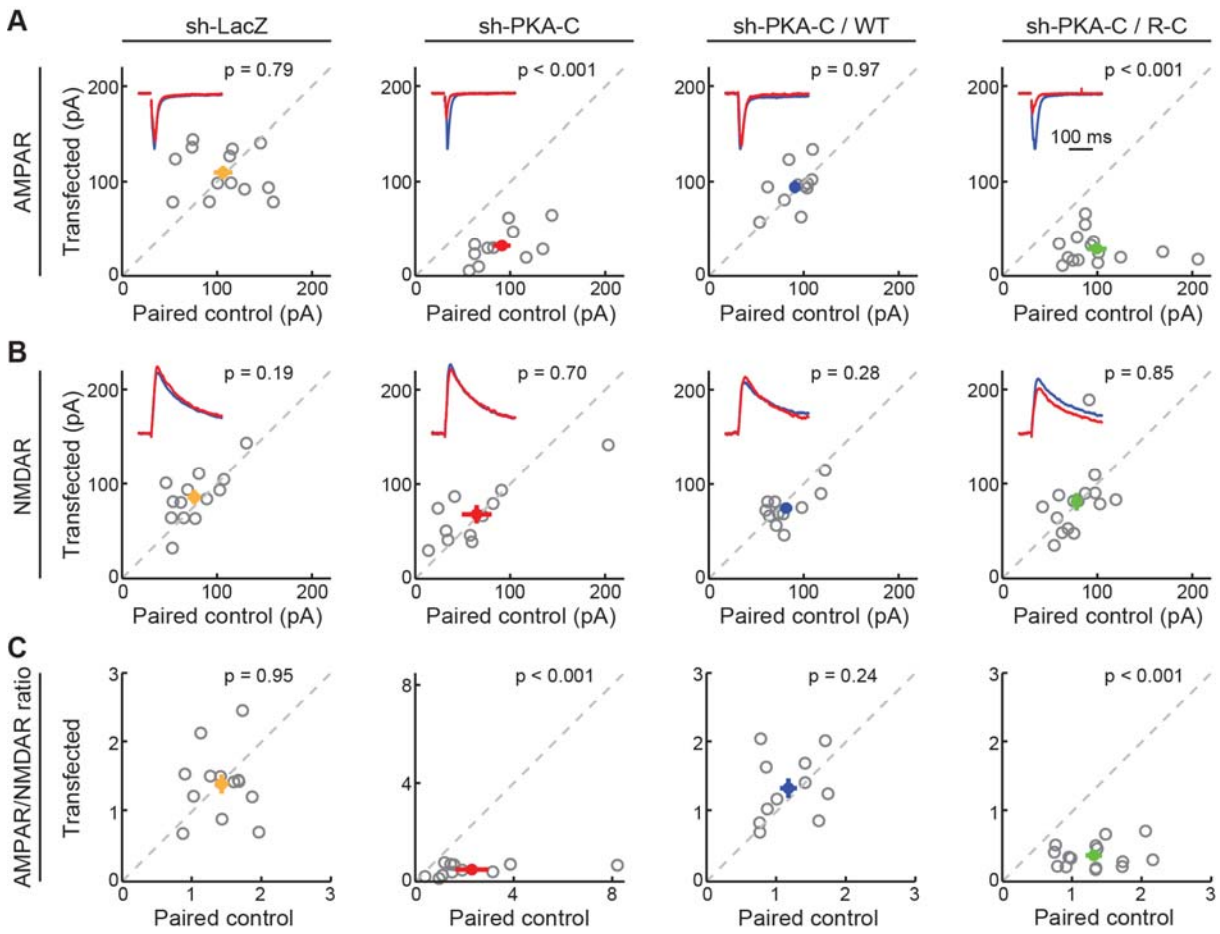

Figure 4. AMPA receptor-mediated synaptic transmission requires wildtype dissociable PKA. (A–C) Representative traces (red) normalized to the paired control (blue) (insets) and scatter plots of paired AMPA (A) and NMDA (B) receptor currents and AMPA/NMDA receptor current ratios (C) from neighboring untransfected CA1 neurons and those transfected with shRNA against PKA-C and the indicated shRNA-resistant rescue constructs. Statistical p values were obtained using a sign test (MATLAB). From left to right, n (neuron pairs) = 13, 11, 11, and 15.

367

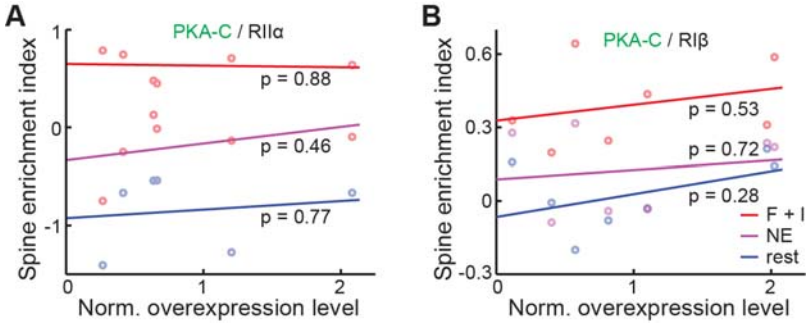

368 **Figure S1**. Spine enrichment indexes and the movement of PKA-C into spines upon

369 activation are not dependent on the protein expression level. (A–B) Averaged spine

370 enrichment indexes within individual neurons of PKA-C co-expressed with RIIα (A) and RIβ

371 (B), and their linear fit at rest or under the indicated stimulation.